MATERIALS PHYSICS AND MECHANICS RESEARCH ARTICLE

Submitted: March 12, 2024 **Revised: June 4, 2024** **Accepted: July 31, 2024**

Structural changes in a commercial Al-Cu alloy during hot equal channel angular pressing

O.S. Sitdikov ✉

Institute for Metals Superplasticity Problems of RAS, Ufa, Russian Federation

✉ sitdikov.oleg@imsp.ru

ABSTRACT

The evolution of the structure of aluminum alloy 2219 ingot during equal channel angular pressing (ECAP) to a cumulative strain of e = 12 at 475 °C (~0.8T_m) was studied. It was found that the structural changes during hot ECAP were determined by the action of two main structural processes. In the early stages of ECAP (e = 1–3), the alignment of the initial grains in the pressing direction was mainly accompanied by the formation of a dynamically equilibrated subgrain structure. However, upon reaching a critical strain (e ≈ 3–4), grain fragmentation by deformation/microshear bands started with a subsequent gradual increase in the number of bands and their misorientation, leading to grain refinement. As a result, a heterogeneous bimodal grain structure was formed after e = 12, consisting of about 50 % new grains of about 10 μm size and residual fragments of the initial grains containing subgrains. It was concluded that grain refinement during hot ECAP occurred by the mechanism of continuous dynamic recrystallization.

KEYWORDS

aluminium alloy 2219 • equal channel angular pressing • ECAP • microstructural evolution • grain refinement

Funding. *The research was supported by the Ministry of Science and Higher Education of the Russian Federation within the framework of the state assignment of IMSP RAS*

Acknowledgements: *The author is grateful to Prof. T. Sakai (UEC Tokyo, Japan) and Drs. A. Belyakov and R. Kaibyshev (BSU, Russia) for fruitful discussions that contributed to this study. Some experimental results were obtained in the joint research with I.A. Mazurina and I.S. Oleneva.*

Citation: Sitdikov OS. Structural changes in a commercial Al-Cu alloy during hot equal channel angular pressing. *Materials Physics and Mechanics*. 2025;53(1): 89–108.
http://dx.doi.org/10.18149/MPM.5312025_8

Introduction

The problem of obtaining bulk ultrafine-grained (UFG) materials (grain size less than 1 μm) is of considerable interest to researchers working in the field of materials science and solid state physics [1–5]. This is due to the range of high physical and mechanical properties that can be achieved, allowing such materials to be widely used in practical applications [2,3]. In order to form a UFG structure in bulk billets, severe plastic deformation (SPD) methods, such as equal channel angular pressing (ECAP) [1–5], accumulative roll bonding [1,2,5], multidirectional isothermal forging [1–3,5], etc. are often used. In addition, these methods can also be considered as an effective "scientific tool" for obtaining knowledge about the structural changes that occur during large strain deformations [1,4,5].

At present, both the characteristics of the above-mentioned SPD methods and the properties of the UFG-structured semi-finished products obtained by such methods have been quite well studied [1–35]. In particular, a large number of studies have been devoted

Publisher: Peter the Great St. Petersburg Polytechnic University

to the analysis of changes in the structure of aluminum alloys, which are typical materials with high stacking fault energy. It has been shown in [4,6,8,12–21,24,26,31] that in these alloys SPD can cause fragmentation of the initial grains with the formation of dislocation boundaries with medium angular misorientation ($\Theta \approx 5–15°$), which are the boundaries of deformation bands. With increasing strain, the number and misorientation of these boundaries increase, leading to the formation of new ultrafine grains surrounded mainly by high-angle boundaries ($\Theta \geqslant 15°$) at relatively high strains. It has been concluded that the formation of new grains in this case is due to the occurrence of continuous dynamic recrystallization (cDRX) [11,12,15,16,21,26].

However, detailed studies of the microstructure evolution during SPD in aluminum and its alloys have usually been limited to the temperature range from 20 to 250–300 °C ($T \leq 0.6T_m$), i.e. they have been performed under conditions of so-called cold or warm deformation [1,4,6–8,10–24,27,28,31]. At the same time, they were carried out much less frequently under conditions of hot deformation at higher temperatures ($T \approx 0.7–0.8T_m$). This can be explained both by the technical difficulties of implementing SPD schemes under isothermal conditions at high temperatures (e.g. in the ECAP process) and by the decrease in practical interest in materials where the size of the resulting grains no longer belonged to the UFG range. Accordingly, the use of SPD schemes at such high temperatures has generally been recommended only for processing hard-to-deform and/or brittle materials. As a result, there remains a significant gap in the understanding of the nature and characteristics of structure formation at large strains and high temperatures [35].

For example, it has been shown in [11,26] that the same grain refinement mechanism associated with grain fragmentation due to deformation banding can occur at different temperatures during both warm and hot deformation. In the case of Al-Mg alloys with transition metals (such as Al 1570) [26], this mechanism led to the formation of new grain structures with similar angular characteristics regardless of processing temperature. In a number of cases, grain refinement accelerated with increasing temperature, particularly in high-strength complex-alloyed alloys of the 7XXX series [12,18]. In other materials, however, an increase in temperature may suppress grain refinement or alter the dominant mechanisms of structure formation, such as in Al, Al-Cu alloys, and some steels [6,9,10,13,16,19,23,29,30,32]. Therewith, possible variants of material behavior during hot deformation were the transition from fragmentation-related cDRX to either geometric-type dynamic recrystallization or discontinuous dynamic recrystallization [13,25,27,29,30]. It has also been suggested that in the high-temperature region, the process of grain refinement due to the development of deformation bands may be replaced by the evolution of more homogeneous deformation-induced subgrain structures associated with the progressive rotation of individual subgrains and their transformation into new grains. Thus, the question of the mechanisms and patterns of new grain formation during hot deformation remains open (and covered by rather insufficient information in the literature).

The objective of this work was to analyze the microstructural changes during ECAP of the aluminum alloy 2219 at 475 °C (about $0.8T_m$). Previous studies [15,16,33] have shown that ECAP at temperatures of 250–475 °C leads to the formation of new grains after high strains ($e = 10–12$). However, the evolution of the microstructure has been

studied in detail mainly during warm deformation at 250 °C [15], while the features of the structural changes at the highest temperature (475 °C) have been insufficiently investigated and only partially presented in previous publications [16,33]. In the present work, additional studies of the microstructure at this temperature as a function of strain were carried out in order to identify the main mechanisms and factors influencing grain refinement during hot working of the aluminum alloy.

Materials and methods

Commercial aluminum alloy AA2219 with the following chemical composition Al-6.4Cu-0.3Mn-0.18Cr-0.19Zr-0.06Fe (wt. %) was produced by the semi-continuous casting method. The alloy was homogenized at a temperature of 530 °C for 6 h, followed by cooling in a furnace to obtain an equilibrium phase composition.

The workpieces for ECAP, in the form of rods 20 mm in diameter and 100 mm in length were cut parallel to the ingot axis. ECAP was performed under isothermal conditions at a temperature of 475 °C using a die with an L-shaped channel configuration with internal and external angles of $\varphi = 90°$ and $\psi = 0°$, respectively. This configuration provided a true equivalent strain e of approximately 1 per pass [6]. The workpieces were deformed to $e = 12$ using the route A (i.e., without rotation between passes). The deformation was performed in a hydraulic press with a ram speed of 6 mm/s. According to [36], this resulted in an average effective strain rate of 3 s^{-1}. To fix the formed microstructure, the pressed parts were cooled in water after each pass and then heated for 45 min before the next pass. The average time interval between the start of deformation in each pass and the immersion of the workpiece in water after pressing was about 1.5 min. Some additional time for the workpiece in the die was due to the typical features of the ECAP process, where the workpiece after pressing is pushed out of the channel by the next workpiece inserted into the die. The structure of the workpieces subjected to ECAP was analyzed in a longitudinal section parallel to the pressing direction (PD).

Metallographic analysis was carried out using optical microscopy (OM) after etching the samples in Keller's standard reagent. For scanning electron microscopy (SEM) with electron backscatter diffraction (EBSD) analysis, the samples were electropolished in a solution of 80 % C_2H_5OH, 12 %, 2n-butoxyethanol, 8 % $HClO_4$ at room temperature. EBSD analysis was performed using Hitachi S-4300H and TESCAN MIRA3 LMH field emission scanning electron microscopes equipped with OIM Analysis™ and HKL Channel 5 software, respectively [37,38]. The investigated areas were scanned with a step size of 1.5 μm. In the EBSD maps of the reconstructed structures, different colors corresponded to different crystallographic orientations according to the standard green (110) / red (100) / blue (111) triangle, and intercrystallite boundaries with low ($2 \leqslant \theta < 5°$), medium ($5 \leqslant \theta < 15°$) and high ($\theta \geq 15°$) angular misorientations were marked with thin white, thin dark gray and thick black lines, respectively. Boundaries with misorientations less than 2° were not considered. Distributions of misorientations of deformation-induced (sub)grain boundaries were obtained from the EBSD data both for the entire scanned area and for selected areas (using the standard "structure cropping" and/or "subset selection" options of the EBSD software [37,38]), as described in more detail below. The average grain size in the formed fine-grained regions was estimated using the line-intercept method. The

width of the deformation bands (the average distance between the nearest band boundaries) was measured perpendicular to the direction of their preferred orientation. The volume fraction of fine grains V_{fg} was determined by the point-counting method. Thin foils for transmission electron microscopy (TEM) were obtained by electropolishing at a temperature of -28°C in a solution of 30 % HNO_3 and 70 % CH_3OH using a TenuPol-5 double-jet polisher and examined with a JEOL 2000EX TEM microscope.

Results and Discussion

Initial structure

After homogenization, the alloy matrix was represented by equiaxed grains with diameters ranging from 100 to 400 μm (Fig. 1(a)). Several types of second phases were identified in the structure [39–41]: T-phase dispersoids ($Al_{20}Cu_2Mn_3$) in the form of plates up to 200 nm long, as well as spherical precipitates of Al_7Cr and Al_3Zr with sizes of 80 and 20 nm, respectively (Fig. 1(b)). Larger precipitates of the main strengthening phase Θ (Al_2Cu) were also observed, uniformly distributed within the grains and in the boundary regions (Fig. 1). It is known that precipitates of the Al_3Zr phase can be both coherent and incoherent with the matrix after homogenization [40]. According to the analysis in [39], almost 90 % of the Al_3Zr dispersoids in the studied alloy were incoherent.

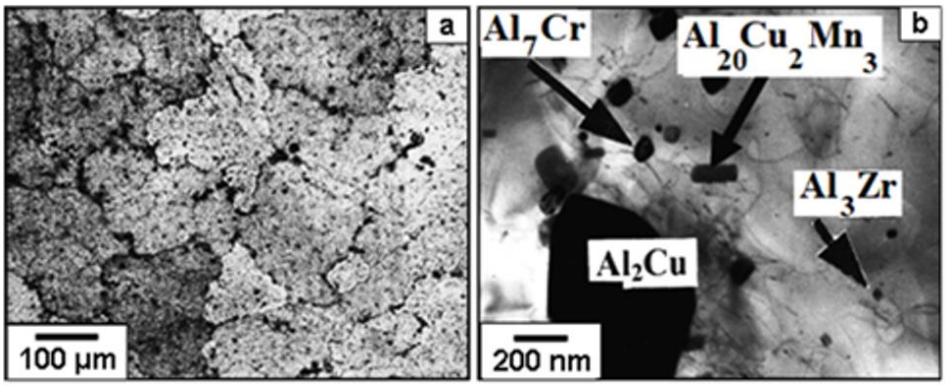

Fig. 1. Initial structure of alloy 2219 after homogenization: (a) OM; (b) TEM

Structure formed during ECAP

A typical alloy structure formed during ECAP is shown in Figs. 2 and 3. At $e \leqslant 4$, pressing along route A mainly resulted in a change in the shape of the initial grains, which were elongated in the pressing direction (PD) according to simple shear [4,5] (Fig. 2(a)). As a result, after $e = 4$ (Fig. 2(b)), a non-uniform microstructure was observed in the material, containing large elongated grains in the interior of which a well-developed substructure was formed, as judged by the etching patterns. In some areas, these grains acquired wavy boundaries (see for example the upper part of Fig. 2(b)) and were sometimes replaced by chains of smaller and more equiaxed crystallites, as can be seen in the attached higher magnification image in the lower left corner of Fig. 2(b).

With a further increase in the number of passes ($e = 4–12$), the character of the microstructural evolution changed significantly (Fig. 3). Namely, new fine grains began

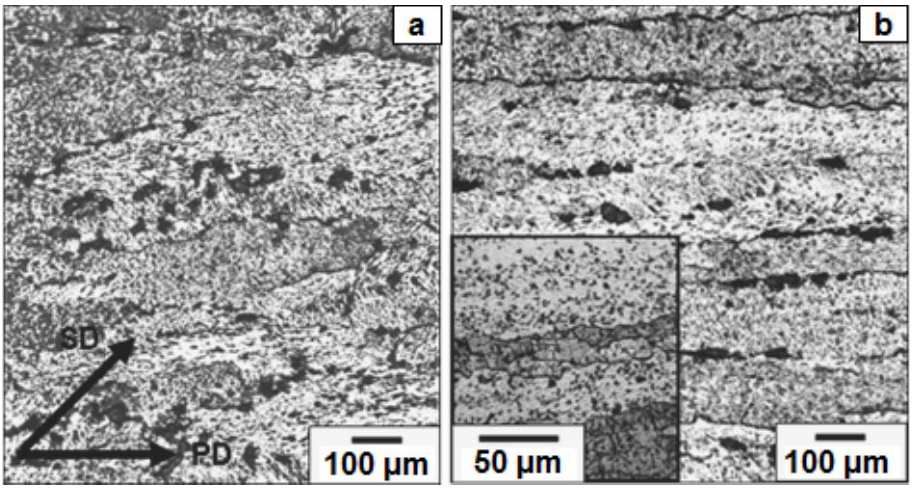

Fig. 2. OM-images of microstructure of alloy 2219 after ECAP at T = 475 °C to: (a) e = 2, (b) e = 4. Hereafter, SD is the main shear direction, PD is the pressing direction during ECAP

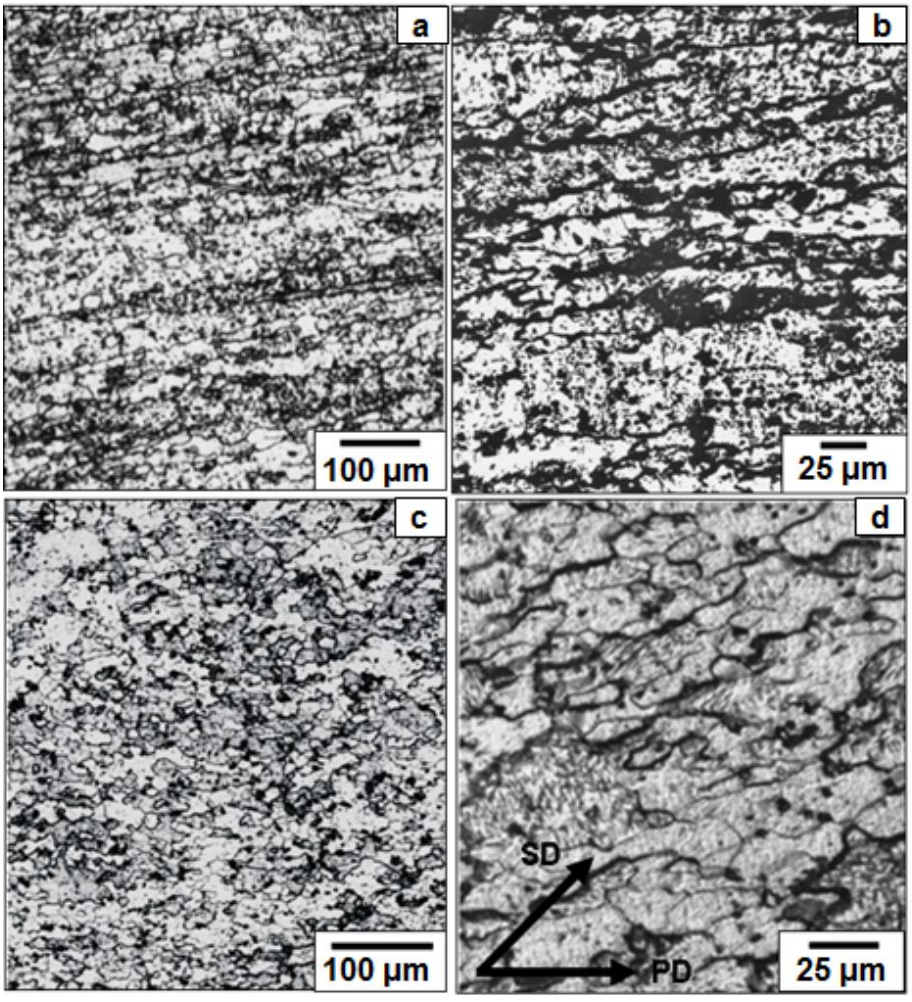

Fig. 3. OM-images of microstructure of alloy 2219 after ECAP at T = 475 °C to: (a,b) e = 8, (c,d) e = 12

to form within the large grains and the coarse-grained microstructure was gradually replaced by regions of a new fine-grained structure. After e = 8–12, a mixed bimodal structure was observed in the alloy, consisting of colonies of fine grains and larger fragments of the initial grains aligned in the PD (Fig. 3(a,c)). At higher magnification it

can be seen that the grains were refined mainly by the formation of banded structures at the mesolevel and fragmentation of the initial grains (Fig. 3(b)). After e = 12, most of the new small grains had an elongated shape and common boundaries within the bands, which were predominantly oriented along the main shear direction (SD) during ECAP, i.e. at an angle of about 45° with respect to the PD (Fig. 3(d)). The observed evolution of the alloy microstructure can be quantitatively characterized by the change in the volume fraction of new fine grains (V_{fg}) during ECAP (Fig. 4). Up to e = 3, V_{fg} did not exceed 5 %, but began to increase rapidly at $e \geqslant 4$. However, even at such a high strain as e = 12, the volume fraction of fine grains reached relatively low values, barely exceeding 50 %.

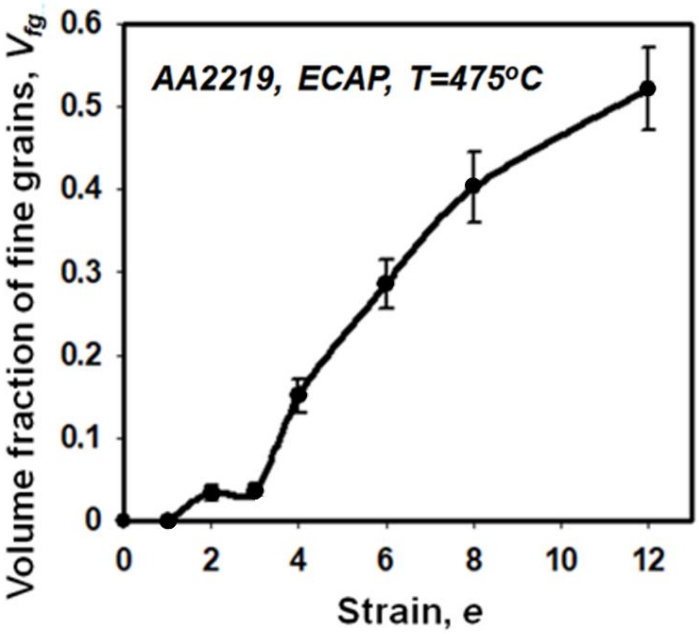

Fig. 4. Strain dependence of the volume fraction of new fine grains formed in alloy 2219 during ECAP at T = 475 °C

EBSD (Figs. 5–7) and TEM (Fig. 8) were used to examine the deformation structures formed during ECAP in more detail. Figure 5 shows that in the early stages of ECAP (e = 1–3), a network of low angle boundaries was formed within the initial grains. These boundaries were uniformly distributed in the matrix and were mainly associated with the formation of a homogeneous subgrain structure due to the occurrence of dynamic polygonization [42–45]. In addition, after e = 1, extended subboundaries with low and medium angular misorientations oriented at angles from 0 to 15° relative to the PD were observed in individual grains (Fig. 5(a)). The formation of these boundaries, as judged by the local change in color contrast within the grains, was accompanied by significant lattice rotations. This allowed them to be classified as deformation bands resulting from strain localization [4,6,17,24,26,34,46].

It is well known that deformation bands can form in a material when fewer than five independent slip systems required for uniform deformation are active [1,17,44–46]. These include the so-called primary deformation bands [14,17,24,34], which show fairly clear boundaries on EBSD maps and can develop at the macro- and mesolevel (i.e. at the level of several initial grains) in the early stages of ECAP. However, it was quite surprising

to observe their formation in an alloy with an fcc lattice at a temperature of $0.8T_m$, when a priori at least five slip systems should be active in most grains. Probably, the formation of deformation bands during hot ECAP was caused by plastic restrictions in some grains due to the requirements of their compatible deformation with neighboring grains [1,11,12,14–17,20,44], which occurred independently of the processing temperature, and/or was a result of deformation localization during ECAP due to the peculiarities of their orientation with respect to the main shear plane [4–6]. It should be noted that after their formation such deformation bands could exist in the alloy even at high temperatures due to stabilization of the dislocation structure by precipitates of second phases [12,21,22,27,43], mainly dispersoids (see Figs. 1 and 8).

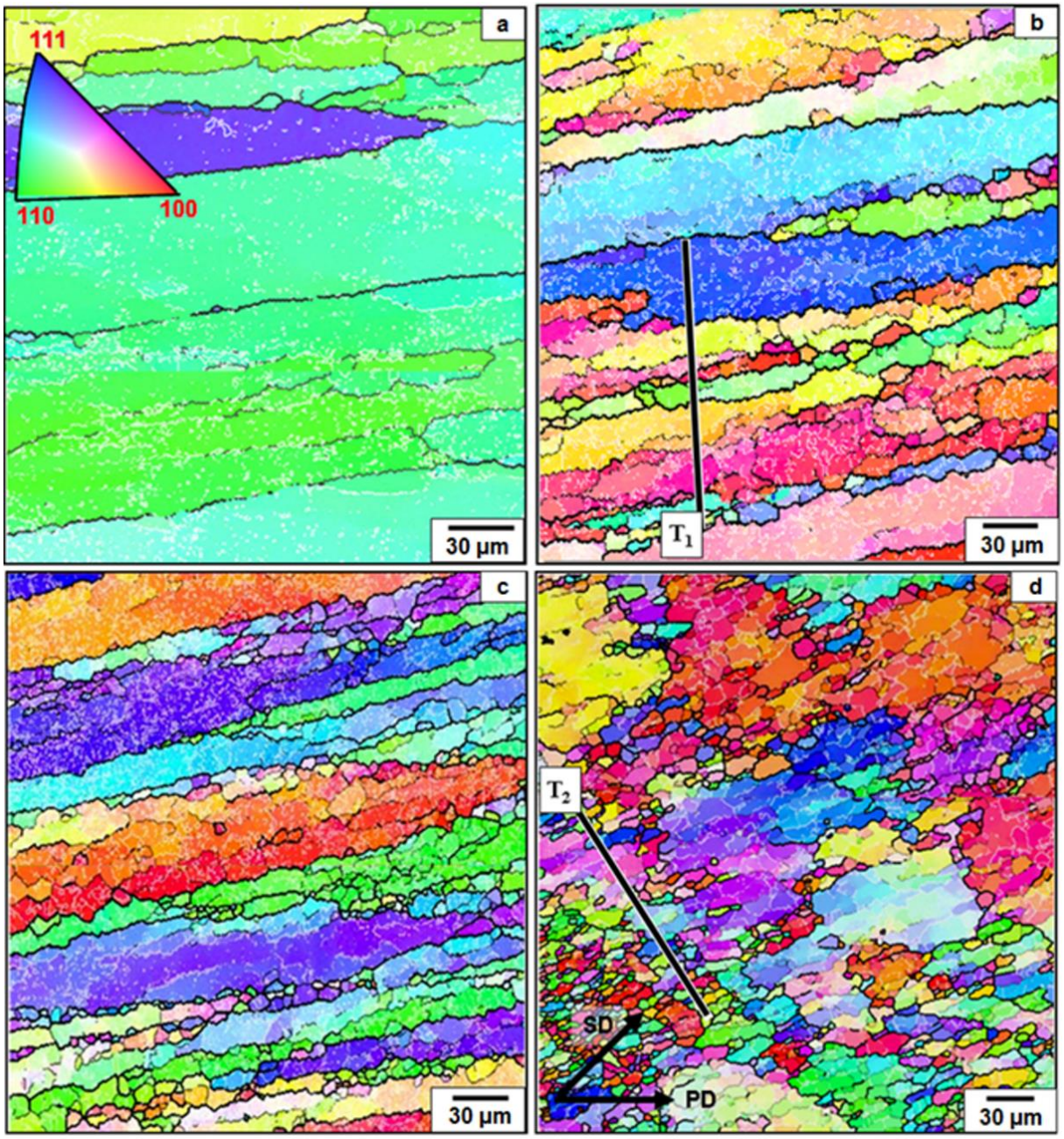

Fig. 5. Typical EBSD maps of alloy 2219 after ECAP at T = 475 °C to: (a) e = 1, (b) e = 2, (c) e =3, (d) e = 6

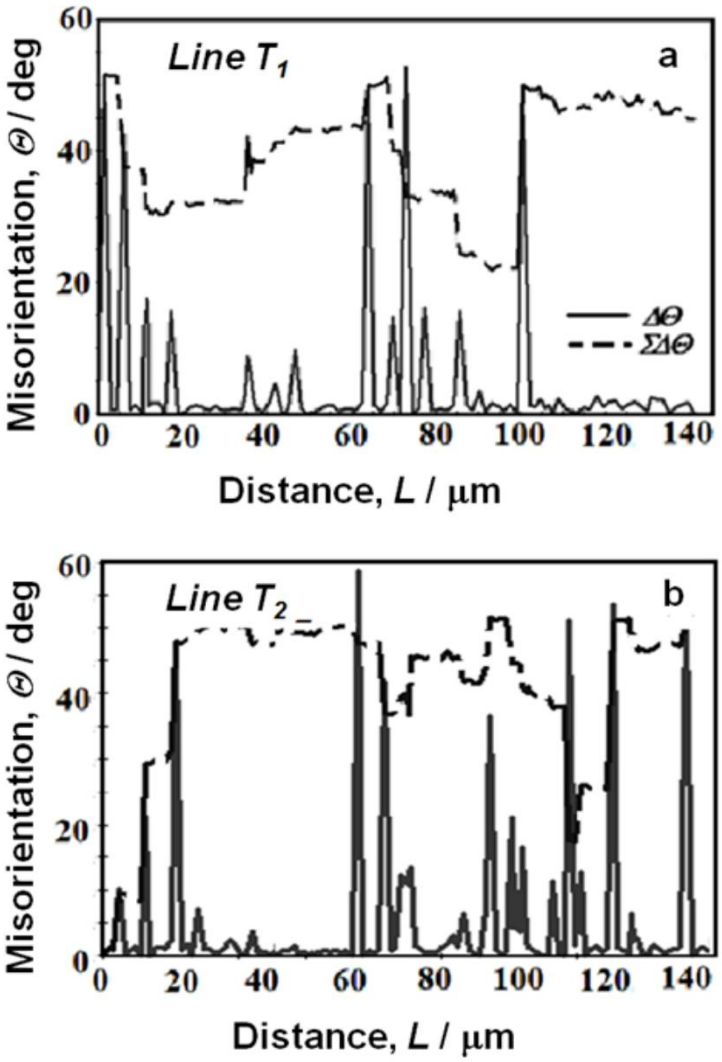

Fig. 6. Change in misorientations between adjacent points (ΔΘ) and relative to the initial point (ΣΔΘ) along test lines T_1 and T_2 in Fig. 5

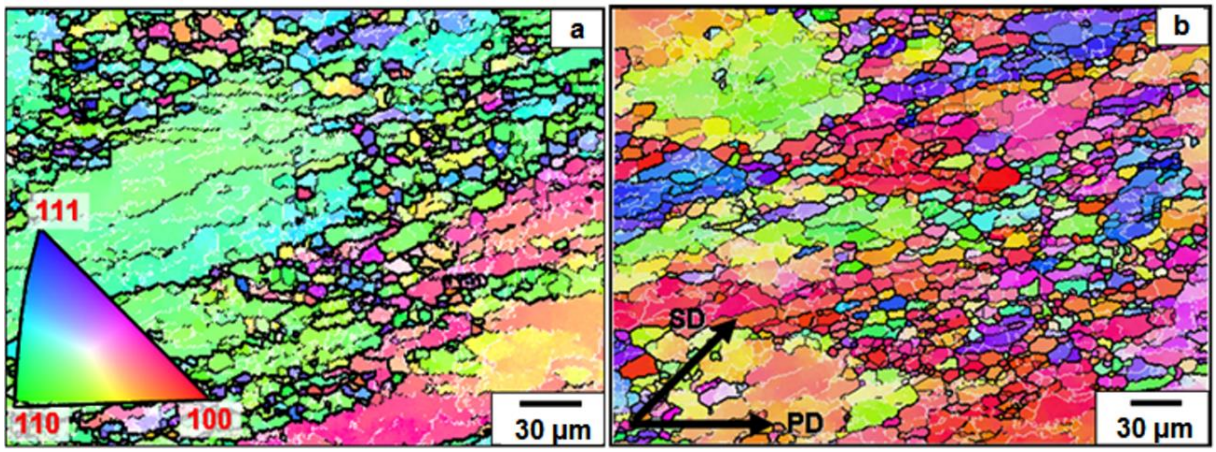

Fig. 7. EBSD maps of alloy 2219 after ECAP at T = 475 °C to: (a) e = 8, (b) e = 12

It is known from the literature that during cold and warm deformation of aluminum alloys, once formed, deformation bands remain permanent elements of the structure, in contrast to cells/subgrains which are of an "incidental" nature [42,44], i.e. they are

continuously repolygonized during deformation. Accordingly, under simple shear during cold ECAP, the band boundaries, like the boundaries of the initial grains, gradually align along the PD with increasing strain, leading to an additional increase in the number of longitudinal intercrystallite boundaries [4,6,8,13,17,21,24,34]. Similar structural changes were observed in the early stages of hot ECAP of this alloy (Fig. 5). Namely, at e = 2–3, single grains containing deformation bands were transformed into fibers elongated along the PD, outlined by alternating longitudinal boundaries of bands with medium to high angular misorientations and boundaries of the initial grains (Fig. 5(b,c)). The width of such crystallites at the strains considered was significantly smaller than the average distance between the longitudinal boundaries of the initial deformation band-free grains [25]. In subsequent passes, the misorientation of the deformation band boundaries increased and the distance between them decreased. Note that some of these thinner fibers were replaced by chains of equiaxed grains with a close (judging by the color contrast on the EBSD maps) crystallographic lattice orientation and approximately the same transverse size as the fibers themselves. This suggests that new grains could form in place of the deformation bands as a result of a mechanism similar to geometric dynamic recrystallization [25,33,42,43]. Thus, during ECAP, the fiber boundaries became serrated (see Figs. 2 and 5) due to the surface tension of the subgrain boundaries formed during dynamic polygonization [43]. As the distance between fiber boundaries decreased during deformation, opposite boundary segments could come into contact and annihilate each other, leaving more equiaxed fine grains in the structure [25,43].

The conclusion about the occurrence of geometric dynamic recrystallization during high-temperature ECAP of the studied alloy was also based on the results of microstructural observations in a previous work [33]. However, from the subsequent detailed study of the transformation of a similar coarse-grained structure during ECAP in another alloy [25], it should be noted that at e < 3–4 the distance between the boundaries of most of the initial grains remains quite large for the widespread implementation of geometric dynamic recrystallization. At such relatively low strains, this mechanism could only take place in single grains containing deformation bands. Accordingly, the fraction of new grains formed by this mechanism was only a few percent (Fig. 4).

Another feature of the deformation structure of this alloy, although not as noticeable in the early stages of pressing, has been associated with grain fragmentation due to the development of deformation bands at a lower scale (within individual grains), such as microshear bands [4,12,17,24,47]. The EBSD analysis data in Fig. 6 illustrate typical distributions of lattice misorientations between neighboring points ($\Delta\Theta$) and relative to the starting point ($\Sigma\Delta\Theta$) along the test lines T_1 and T_2 drawn within several initial grains in Fig. 5(b) (for e = 2) and Fig. 5(d) (for e = 6), respectively. Figure 6(a) shows that the misorientation values at e = 2 vary mainly randomly from 2 to 5°, corresponding to the intersection of line T_1 with uniformly distributed subgrain boundaries [42–44]. Some peaks with $\Delta\Theta$ greater than 40°, located at a distance of about 40–60 μm from each other, may correspond to the boundaries of the initial grains.

Note, however, that in some regions within the grains, the misorientations reached modal values from 5 to ⩾ 15° with an average spacing between them of about 10–20 μm, and the cumulative misorientation in the same regions changed discontinuously within 10–15°. These peaks indicated the formation of deformation band boundaries similar to

microshear bands, resulting in "rigid" local rotations and shears in the crystal lattice [6,12,17,24,46,47]. The TEM results also support these data. Figure 8(a) shows that at e = 2, elongated crystallites of a non-equilibrium, almost rectangular shape are formed in the material, which may be a consequence of the formation and mutual crossing of the boundaries of the deformation bands [34]. Figure 8(b), taken at a higher magnification, shows that the formation of some such boundaries causes significant displacements and shears in the forming dislocation structure. It can therefore be concluded that these boundaries are the boundaries of microshear bands that develop on the micro- and mesoscale and lead to fragmentation of the initial grains even in the second ECAP pass [17,24,34].

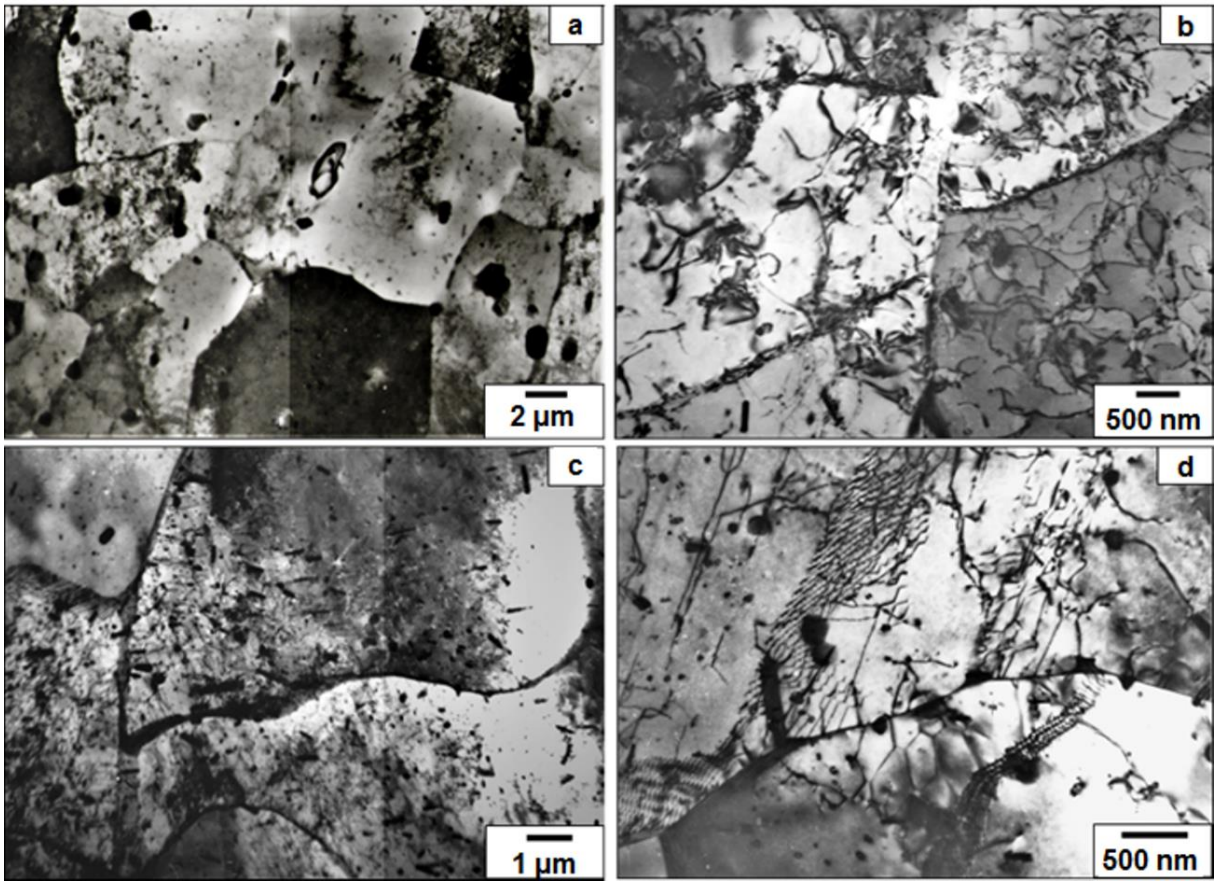

Fig. 8. Typical fine structure of alloy 2219 after ECAP at T = 475 °C to: (a,b) e = 2, (c,d) e = 12

As shown in Fig. 6(b), the number and misorientation of the medium-angle boundaries increased somewhat with increasing strain. Therewith, the EBSD maps clearly showed deformation/microshear bands oriented parallel to SD (i.e. at an angle of 45° to PD), which became one of the main features of the substructure at e = 6 (see Fig. 5(d)). Note that such behavior of the alloy is characteristic of lower deformation temperatures [17,24,34]. Thus, during cold or warm ECAP, microshear bands were formed within the grains regardless of their initial crystallographic orientation [15,17,21,24,34]. In this case, the formation of microshear bands acted as the main structural prerequisite for introducing significant misorientations into the interior of the grains and led to their refinement [17,34,47]. As a result, new grains were formed by fragmentation of the initial

grains during mutual intersection of microshear bands with a subsequent increase in their number and boundary misorientation [12,15].

It has been suggested that the formation of shear bands may be due to a complex interaction of crystal lattice defects and is associated with the involvement of as-formed dislocation structures (lamellar and/or cellular banded) in the ongoing deformation [24,34,48,49]. Accordingly, the development of microshear bands (with subsequent grain refinement) could begin only after certain strains are reached, when stress concentration and/or localization of plastic flow would be sufficient to create such heterogeneous structures. It can be assumed that during hot deformation of this alloy, when the plastic flow was relatively uniform at the micro- and mesolevel during the initial ECAP passes, the formation of microshear bands and grain fragmentation occurred only in localized areas, without being noticeable throughout the sample (Figs. 2,4,5(a–c)). Therefore, only weak signs of strain localization and grain refinement were observed in the range $1 < e < 4$. Accordingly, considering only this strain range, it could be concluded that the main process of structure formation during hot deformation of aluminum alloy is the formation of dynamically equilibrium subgrain structure [43–45].

Meanwhile, the results of this work showed that the formation of new fine grains under the present deformation conditions was simply "delayed" until $e \geqslant 4$, i.e., until microshear bands began to develop extensively in the alloy structure. Thus, in Fig. 5(d), it is evident that at $e = 6$ new fine grains were formed along the deformation/microshear bands oriented in the SD. And with further deformation to $e = 8–12$ (Fig. 7), these grains continued to appear following the propagation and development of the bands, i.e. new grains were formed in fragmented regions at the intersection of the bands. In other regions of the material, where deformation bands practically did not form, low-angle (subgrain) boundaries prevailed (see the segment on line T_2 at a distance of 20 to 60 μm, left side of Fig. 6(b)). In this case, individual large fragments of the initial grains containing subgrains remained even at large strains (Fig. 7(b)).

It should be noted that even at such a high strain as $e = 12$, the fine structure of the alloy revealed by TEM still contained crystallites of predominantly non-equilibrium rectangular shape with angles in triple junctions close to 90° (Fig. 8(c,d)). The formation of such crystallites, as at lower strains, was apparently caused by the intersection of deformation bands. Strong interaction of deformation-induced boundaries and lattice dislocations with second phase particles present in the alloy was also observed. As mentioned above, the latter could effectively restrict the migration of boundaries and the rearrangement of dislocations over large distances, preventing the relaxation of the accumulated deformation energy and thereby creating conditions for the formation of a new fine-grained structure even during hot deformation. On the other hand, the observed curved/wavy grain boundaries (Fig. 8(c)) and the formation of flat dislocation walls inside the grains (Fig. 8(d)) indicated that due to the high rate of diffusion processes during high temperature ECAP, limited grain boundary migration and dislocation rearrangement over short distances often occurred. Such processes facilitated the rapid transformation of deformation band boundaries from dislocation walls to more balanced and flat high angle boundaries and the formation of new fine grains with more equiaxed shape [34].

Analysis of microstructural parameters

Figure 9 shows the minimum width of deformation bands and the average size of new grains[1] formed in fine-grained regions as a function of strain. The width of the deformation bands was measured from the profiles of misorientations along the test lines plotted on the EBSD maps perpendicular to these bands, as the average distance between neighboring boundaries with misorientations from 5 to 15° (see e.g. Fig. 6). Both parameters quickly decreased to $e = 6$ and remained approximately constant at high strains, slightly exceeding 10 μm. The grain size was close to the width of the bands, indicating that the formation of new grains at high strains was mainly controlled by the evolution of the deformation bands. In other words, the formation of new grains was associated with the fragmentation of the initial grains due to the formation of deformation bands and/or microshear bands and their subsequent transformation into new grains [12,15].

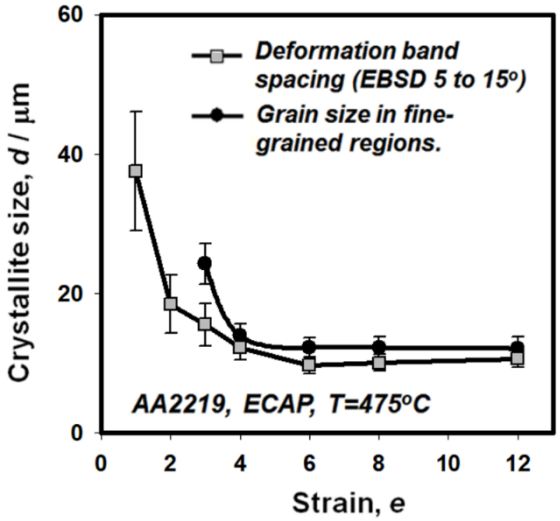

Fig. 9. Strain dependencies of the crystallite size and the width of deformation bands measured in different regions of alloy 2219 after ECAP at $T = 475$ °C

Changes in the distribution of intercrystallite boundary misorientations averaged over all regions of the forming deformation structures (i.e. obtained from the entire EBSD maps) are shown in Fig. 10 depending on strain. The plots of the dependence of the angular parameters of the structure, such as the average misorientation of the crystallite boundaries, Θ_{av}, and the fraction of high angle boundaries, f_{HABs}, are shown in Fig. 11 and are denoted by white squares and dotted lines. At $e = 1–4$ (Fig. 10(a–c)), the misorientation spectra were characterized by the maximum boundary distribution density in the low and medium angle ranges up to 15°, and the high angle misorientations in these spectra apparently corresponded mainly to the boundaries of the initial grains. In this case, the evolution of the primary deformation bands undoubtedly had an additional effect on the misorientation spectrum, causing some shift of their average values towards larger angles.

[1] The grain size was determined at $e \geqslant 3$, since at lower strains the deformation-induced crystallites revealed by EBSD were not completely surrounded by high-angle boundaries (see Fig. 5).

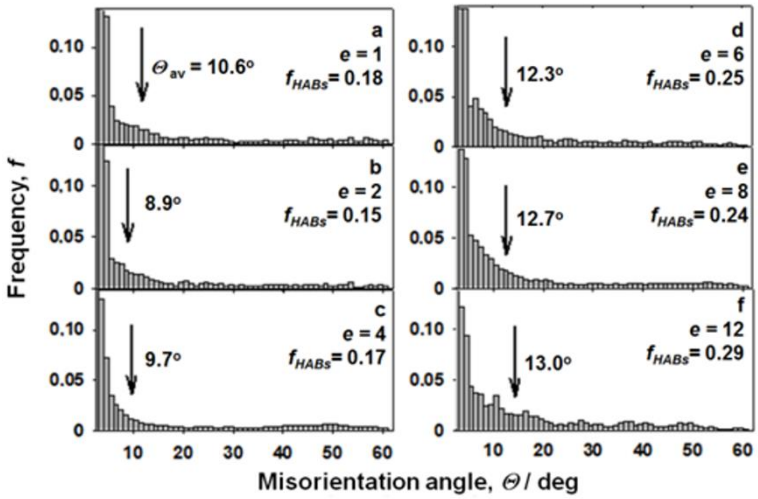

Fig. 10. Changes in the distribution of misorientations of (sub)grain boundaries developing in the structure of alloy 2219 during ECAP at T=475 °C

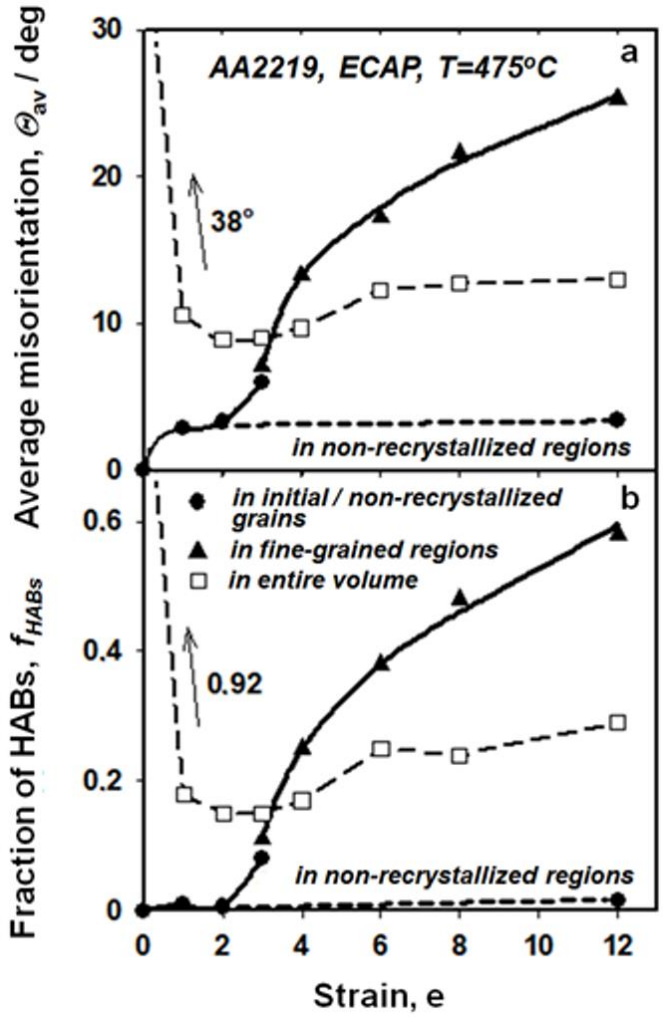

Fig. 11. Changes in (a) the average misorientation of deformation-induced boundaries and (b) the fraction of high-angle boundaries (HABs) formed in different regions of alloy 2219 during ECAP at *T* = 475 °C

However, this practically did not change the shape of the obtained dependencies, since in the early stages of deformation a large number of low angle boundaries were

simultaneously formed in the initial grains, which generally led to a sharp decrease in the average crystallite boundary misorientation and the fraction of high angle boundaries (Fig. 11). At strains $e > 4$, the fraction (fractional density) of medium angle boundaries increased, a new peak appeared in the distributions at 5° (Fig. 10(d)), while the spectrum of misorientations expanded towards larger angles (Figs. 10(d,e)), which was accompanied by an increase in Θ_{av} and f_{HABs} (Fig. 11). This was associated with the intense formation of microshear bands and new grains. However, the angular parameters of the whole structure increased slowly, and at strains $e = 6–12$ a tendency to "saturation" of Θ_{av} and f_{HABs} was observed at relatively low values of about 13° and 0.30, respectively.

At the same time, it seems that the change in the average values of the angular parameters of the microstructure calculated for the entire volume of the material does not always adequately reflect the physical nature of the processes occurring. This is due to the heterogeneity of the structure of the material, which leads to significant differences in the data obtained from different regions, making the use of averaged parameters for the assessment of structural changes ineffective. For example, in a number of studies in the initial stages of SPD, as well as in this alloy, a decrease in the average values of the angular parameters of the structure calculated for the entire volume of the material was observed. However, to the best of the author's knowledge, the corresponding mechanisms of structure formation leading to a decrease in (sub)grain boundary misorientation during deformation have not yet been identified [35]. The decrease in the mean values occurred only due to the formation of a large number of new low angle boundaries in the original polycrystal and was the result of averaging their misorientations with the misorientations of the boundaries of the initial grains. It should be noted that the nature of the dependence of the angular parameters of the structure on the deformation in the early stages of SPD has not yet been determined. Some researchers extrapolate the graphs of $\Theta_{av}=f(e)$ dependencies to zero values, representing a straight line (without any experimental confirmation) directly proportional to the growth of misorientations at the early stages of deformation [29,45]. However, this approach seems to be too simple.

The deformation microstructures in alloy 2219, even at $e = 12$, remained mixed and belonged to two main types:

1. colonies of fine grains, mainly with high angle boundaries;
2. fragments of deformed initial grains containing subgrains.

Therefore, for a more objective analysis of the data obtained from the EBSD maps, it was advisable to analyze their evolution separately in each of the developing regions.

First, the internal regions of large initial grains were identified and analyzed using standard software procedures for EBSD analysis [37,38]. This allowed the influence of initial boundaries and developing deformation bands on the microstructure parameters to be excluded. In this case, the misorientation spectra at strains $e < 3$ also showed maxima at angles less than 5° (Fig. 12(a,b)), but without contributions from grain boundary misorientations in the high angle region. This resulted in constant "low angle" values of microstructural parameters, forming a "plateau" [2] at $\Theta_{av} \approx 3.0–3.5°$ and $f_{HABs} \approx 0$

[2] In a number of studies [11,12,18,19] such "plateaus" can also be observed in the "averaged over all regions" dependence of the structural parameters of alloys in which the initial grain size was relatively large and/or the subgrain size was relatively small, and accordingly the contribution of the initial grain boundaries to the average values of the developing microstructural parameters was not as sensitive.

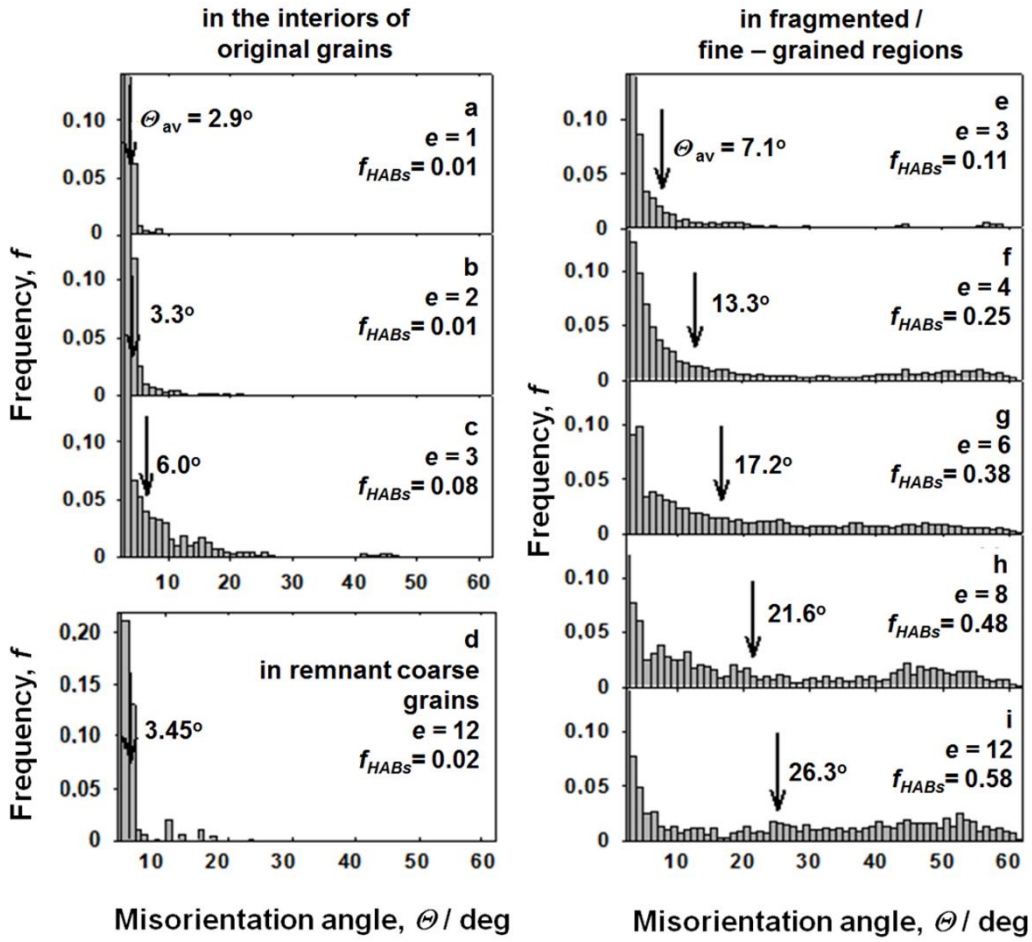

Fig. 12. Distributions of misorientations of (sub)grain boundaries formed in different regions of alloy 2219 during ECAP at T = 475 °C: (a–c) inside the initial grains (e = 1–3); (d) inside the remnant non-recrystallized grains (e = 12); (e-i) in fragmented/fine-grained regions (e = 3–12)

in the early stages of deformation (see graphs indicated by black circles and solid lines in Fig. 11). Contrary to the average characteristics of the microstructure, these plateaus obtained for the “selected” structure could be associated with a certain "incubation period" preceding the formation of new grains [11,12].

Figure 5 shows that the plateaus obtained are mainly related to the formation of a subgrain structure. This structure, similar to the cellular structures formed during cold deformation [4,17,24], can be classified as an "incidental" structure [43]. However, it should be noted that this structure is one of the most characteristic in the early stages of ECAP of this alloy, so its analysis can be important in understanding and describing the characteristics of the structural behavior during high temperature SPD.

It can be assumed that this structure corresponds to the so-called dynamic equilibrium subgrain structure, formed during "conventional" warm or hot deformation of materials with high stacking fault energy as described in [42,44,45]. Microstructural observations [42–45] have shown that these materials undergo dynamic recovery (polygonization) rather than dynamic recrystallization during high temperature deformation. In the early stages of deformation, the rates of formation and annihilation of defects in the crystal structure gradually equalize and a dynamic equilibrium is

reached, leading to a "steady-state" of plastic flow when the parameters of the (sub)grain structure do not further change. However, it should be noted that most traditional deformation schemes, such as rolling or compression, limit the maximum relative strain to about 90–95 %, which corresponds to e = 2.5–3.0. Therefore, comparing these values with the data presented in Figs. 10–12, it can be assumed that studies of the structural behavior of some materials with high stacking fault energy have only been performed at strains within the limits indicated by the plateau. In other words, before noticeable changes at the grain structure level begin to occur in the material (Fig. 4). This suggests that grain refinement at high temperature in some aluminum alloys requires higher strains, which is only possible with SPD.

For example, after the critical strain e = 2–3 was exceeded, medium angle boundaries began to form along with subgrain boundaries in alloy 2219 (Fig. 12(c)). This was accompanied by a rapid increase in Θ_{av} to medium angle values (Fig. 11) and a more than twofold decrease in the distance between deformation bands (Fig. 9). The latter suggests that in the midst of the development of a dynamically equilibrium subgrain structure at the indicated strains, localization of plastic flow occurred, leading to the intensive formation of new deformation bands, which caused fragmentation of the initial grains containing subgrains (Figs. 5–8).

On the other hand, misorientation distributions similar to those shown in Fig. 12(a,b) were also obtained by analyzing the structure developing in the inner parts of large fragments of the initial grains retained in the alloy even at e = 12 (Figs. 11 and 12(d)). The graphs marked with black round dots and dashed lines in Fig. 11 show that the fraction of high-angle boundaries and the average misorientation angle of intercrystallite boundaries in these grains after high strains remained approximately the same as in the early stages of ECAP, i.e. about zero and 3–4°, respectively. This indicates that in the absence of grain fragmentation and refinement during deformation banding, the subgrain structure with low-angle boundaries remains dominant (dynamically balanced and stable) throughout the SPD process and does not transform into a new grain structure even at very high strains. Thus, strain localization and deformation banding is a necessary condition for the formation of new fine grains.

It is noteworthy that at high temperature, the plastic deformation proceeded uniformly, and high deformation gradients did not develop in the remaining large fragments due to the weak influence of the surrounding fine-grained matrix. In this matrix, the deformation energy was almost dissipated due to dynamic recovery and grain boundary sliding [11,12]. At the same time, the subgrains in the remaining fragments corresponded to the "dynamically equilibrium subgrain structure" that was formed in the early stages of plastic flow and maintained its "dynamically equilibrium" state in all areas with relatively uniformly progressing deformation.

In turn, the misorientation spectra obtained for the fragmented/fine-grained regions often showed peaks corresponding to low and medium angle boundaries with misorientations from 2 to 10° (Fig. 12(e,f)) in the early stages of deformation, which gradually expanded to higher angles with increasing strain amidst a noticeable decrease in the fraction of medium angle boundaries (Figs. 12(g–i)). This indicates that the medium angle boundaries (of microshear bands) introduced into the structure were predominantly transformed into boundaries of new grains. It should be noted that the values of the

average misorientation and the fraction of high angle boundaries in the fragmented/fine-grained regions increased significantly faster with increasing deformation, reaching higher values (Θ_{av} = 25° and f_{HABs} = 0.6) at e = 12 (see graphs represented by black triangles and solid lines in Fig. 11) than in the whole material.

At the same time, the dependencies of the angular microstructural parameters on the deformation in the fragmented/fine-grained regions at the studied temperature of 475 °C were close to the dependencies previously obtained for the same alloy at lower ECAP temperatures of 250 and 300 °C, when new ultrafine grains were formed practically throughout the volume of the material [15,16]. This allows us to assume that the same grain refinement mechanism operated in the alloy regardless of the deformation temperature, associated with the localization of deformation and the formation of deformation bands with the subsequent formation of new grains [4,6,17,34,48]. However, the rate and completeness of this process depended on the deformation temperature. At higher temperatures, more uniform dislocation slip (controlled by their climb) and higher rates of dynamic recovery led to the formation of deformation bands in a smaller volume of the material and their development at higher strains [27,50]. Consequently, a smaller number of new grains were formed in the alloy at the same strains. Thus, it can be concluded that grain refinement during SPD of this alloy was controlled by both athermal processes, such as mechanically induced local lattice rotations and deformation banding, and thermally activated processes associated with homogenization of dislocation slip and acceleration of dynamic recovery with increasing temperature.

Another important conclusion from the analysis of the microstructural parameters (Figs. 4,9 and 11) was that the size of the new crystallites formed in place of microshear bands remained practically constant at medium and high strains, while the misorientation of their boundaries gradually increased. Thus, the crystallites formed during deformation increased their misorientation and were transformed *in-situ* into new fine grains without any noticeable growth. It is known that such features of structure evolution are characteristic of deformation-induced continuous reactions of the cDRX type [44]. Thus, it can be argued that the formation of new grains during hot ECAP of this 2219 aluminum alloy, as well as in a number of other aluminum alloys during high-temperature SPD [11,12,26,44], occurred as a result of cDRX.

Conclusions

In this paper, the microstructure evolution of cast aluminum alloy 2219 (Al-6.4Cu-0.3Mn-0.18Cr-0.19Zr-0.06Fe (wt. %)) was investigated during ECAP by route A at 475°C (~0.8T_m) to a total strain of e = 12. The main results can be summarized as follows.

1. The OM data showed that after hot deformation up to strains of e = 4, the alloy structure mainly contained large initial grains aligned in the pressing direction according to the simple shear scheme. At higher strains, new fine grains started to form and the coarse-grained microstructure was gradually replaced by a mixed bimodal structure consisting of fine grains and larger fragments of the initial grains. The size and volume fraction of new grains in such a structure at e = 12 were about 10 μm and 50 %, respectively. The results obtained indicate the need to achieve large strains to refine the grains during hot working of this alloy.

2. SEM and TEM studies, including electron backscatter diffraction analysis, showed that the main structural changes in the early stages of ECAP (e = 1–2) were associated with the formation of a nearly homogeneous "dynamically equilibrium" subgrain structure with low-angle boundary misorientation ($\theta < 5°$) inside the grains. Its formation was due to homogeneous slip and dislocation rearrangement typical of hot deformation of aluminum alloys under conditions of high dynamic recovery rate. This structure was maintained inside the non-recrystallized grains over the whole range of strains studied, giving an approximately constant average misorientation of the intercrystallite boundaries of 3–4°.
3. Grain refinement during high-temperature ECAP was associated with the development of non-uniform deformation, leading to the formation of various types of deformation bands with medium-angle ($5 \leq \theta < 15°$) misorientation of boundaries against the background of the equilibrium subgrain structure. Thus, as a result of deformation localization at the macro/meso level in the initial stages of ECAP, primary deformation bands oriented at an angle of up to 10–15° to the pressing axis developed in some initial grains. With further deformation, they increased their misorientation to high-angles ($\theta \geq 15°$) and were aligned along the pressing axis together with the initial grains. This resulted in a rapid decrease in the distance between high-angle boundaries in the transverse direction in some grains, followed by the onset of geometric dynamic recrystallization.
4. Another and more pronounced mechanism of grain refinement was associated with microshear bands oriented along the shear plane during ECAP, which were formed after the critical strain of about e = 2–3. During the subsequent ECAP, a gradual refinement of the initial grains occurred by the mechanism of their fragmentation, where new fine grains were formed by mutual intersection of microshear bands developed in different passes, with a subsequent increase in their number and misorientations. This led to the formation of a microstructure with an average misorientation of the intercrystallite boundaries of about 23°.
5. Analysis of the dependence of the microstructural parameters on strain showed that grain refinement in alloy 2219 during hot ECAP occurred by the mechanism of cDRX.

CRediT authorship contribution statement

Oleg Sh. Sitdikov: writing – review & editing, writing – original draft.

Conflict of interest

The author declares that he has no conflict of interest.

References

1. Humphreys FJ, Prangnell PB, Bowen JR, Gholinia A, Harris C. Developing stable fine-grain microstructures by large strain deformation. *Philosophical Transactions of the Royal Society A: Mathematical Physical and Engineering Sciences*. 1999;357(1756): 1663–1681.
2. Edalati K, Bachmaier A, Beloshenko VA, Beygelzimer Y, Blank VD, Botta WJ, Bryła K et al. Nanomaterials by severe plastic deformation: Review of historical developments and recent advances. *Materials Research Letters*. 2022;10(4): 163–256.
3. Mulyukov RR, Imayev RM, Nazarov AA, Imayev MF, Imayev VM. *Superplasticity of ultrafine grained alloys: Experiment, theory, technologies*. Moscow: Nauka; 2014. (In Russian)

4. Beyerlein IJ, Tóth LS. Texture evolution in equal-channel angular extrusion. *Progress in Materials Science.* 2009;54(4): 427–510.
5. Segal V. Review: Modes and processes of severe plastic deformation (SPD). *Materials.* 2018;11(7): 1175.
6. Segal V. Equal channel angular extrusion: from macromechanics to structure formation. *Materials Science and Engineering: A.* 1999;271(1–2): 322–333.
7. Yamashita A, Yamaguchi D, Horita Z, Langdon TG. Influence of pressing temperature on microstructural development in equal-channel angular pressing. *Materials Science and Engineering: A.* 2000;287(1): 100–106.
8. Gholinia A, Prangnell PB, Markushev MV. The effect of strain path on the development of deformation structures in severely deformed aluminium alloys processed by ECAE. *Acta Materialia.* 2000;48(5): 1115–1130.
9. Chakkingal U, Thomson PF. Development of microstructure and texture during high temperature equal channel angular extrusion of aluminium. *Journal of Materials Processing Technology.* 2001;117(1–2): 169–177.
10. Wang YY, Sun PL, Kao PW, Chang CP. Effect of deformation temperature on the microstructure developed in commercial purity aluminum processed by equal channel angular extrusion. *Scripta Materialia.* 2004;50(5): 613–617.
11. Goloborodko A, Sitdikov O, Kaibyshev R, Miura H, Sakai T. Effect of pressing temperature on fine-grained structure formation in 7475 aluminum alloy during ECAP. *Materials Science and Engineering: A.* 2004;381(1–2): 121–128.
12. Sitdikov O, Sakai T, Goloborodko A, Miura H, Kaibyshev R. Grain refinement in coarse-grained 7475 Al alloy during severe hot forging. *Philosophical Magazine.* 2005;85(11): 1159–1175.
13. Popovic M, Verlinden B. Microstructure and mechanical properties of Al–4·4 wt-%Mg alloy (AA5182) after equal channel angular pressing. *Materials Science and Technology.* 2005;21(5): 606–612.
14. Werenskiold JC, Roven HJ. Microstructure and texture evolution during ECAP of an AlMgSi alloy: Observations, mechanisms and modeling. *Materials Science and Engineering: A.* 2005;410–411: 174–177.
15. Mazurina I, Sakai T, Miura H, Sitdikov O, Kaibyshev R. Grain refinement in aluminum alloy 2219 during ECAP at 250°C. *Materials Science and Engineering: A.* 2008;473(1–2): 297–305.
16. Mazurina I, Sakai T, Miura H, Sitdikov O, Kaibyshev R. Effect of deformation temperature on microstructure evolution in aluminum alloy 2219 during hot ECAP. *Materials Science and Engineering: A.* 2008;486(1–2): 662–671.
17. Huang Y, Prangnell PB. Orientation splitting and its contribution to grain refinement during equal channel angular extrusion. *Journal of Materials Science.* 2008;43(23–24): 7273–7279.
18. Sitdikov O, Sakai T, Miura H, Hama C. Temperature effect on fine-grained structure formation in high-strength Al alloy 7475 during hot severe deformation. *Materials Science and Engineering: A.* 2009;516(1–2): 180–188.
19. Mazurina I, Sakai T, Miura H, Sitdikov O, Kaibyshev R. Partial grain refinement in Al-3%Cu alloy during ECAP at elevated temperatures. *Materials Transactions.* 2009;50(1): 101–110.
20. Subbarayan S, Roven HJ, Chen YJ, Skaret PC. Microstructure evolution in pure aluminium processed by equal channel angular pressing at elevated temperature. *International Journal of Materials Research.* 2013;104(7): 630–636.
21. Sitdikov O, Avtokratova E, Sakai T. Microstructural and texture changes during equal channel angular pressing of an Al–Mg–Sc alloy. *Journal of Alloys and Compounds.* 2015;648: 195–204.
22. Gazizov M, Malopheyev S, Kaibyshev R. The effect of second-phase particles on grain refinement during equal-channel angular pressing in an Al–Cu–Mg–Ag alloy. *Journal of Materials Science.* 2015;50(2): 990–1005.
23. Shaeri MH, Shaeri M, Ebrahimi M, Salehi MT, Seyyedein SH. Effect of ECAP temperature on microstructure and mechanical properties of Al–Zn–Mg–Cu alloy. *Progress in Natural Science: Materials International.* 2016;26(2): 182–191.
24. Huang Y. Substructural alignment during ECAE processing of an Al-0.1Mg aluminium alloy. *Metals.* 2016;6(7): 158.
25. Sitdikov OSh. Microstructure evolution in high-temperature equal channel angular pressing of Al-3% Cu alloy. *Physical Mesomechanics.* 2017;20(2): 95–109.
26. Sitdikov O, Garipova R, Avtokratova E, Mukhametdinova O, Markushev M. Effect of temperature of isothermal multidirectional forging on microstructure development in the Al-Mg alloy with nano-size aluminides of Sc and Zr. *Journal of Alloys and Compounds.* 2018;746: 520–531.
27. Sitdikov OS, Avtokratova EV, Zagitov RR, Markushev MV. Influence of the temperature of equal-channel angular pressing on fine-grain structure formation in the alloy Al-3% Cu. *Letters on Materials.* 2021;11(3): 332–337.
28. Baig M, Seikh AH, Rehman AU, Mohammed JA, Hashmi FH, Ragab SM. Microstructure evaluation study of Al5083 alloy using EBSD technique after processing with different ECAP processes and temperatures. *Crystals.* 2021;11(8): 862.
29. Yanushkevich Z, Belyakov A, Kaibyshev R. Microstructural evolution of a 304-type austenitic stainless steel during rolling at temperatures of 773–1273K. *Acta Materialia.* 2015;82: 244–254.

30. Gholizadeh R, Terada D, Shibata A, Tsuji N. Strain-dependence of deformation microstructures in ultra-low-C IF steel deformed to high strains by torsion at elevated temperatures. *Nano Materials Science*. 2020;2(1): 83–95.
31. Jagadeesh C, Shivananda NH, Ramesh S, Praveen TR. Effect of multi-directional forging on the evolution of microstructural and mechanical properties of lightweight Al-Cu-Li alloy AA2050. *Journal of Materials Engineering and Performance*. 2023;32: 11118–11132.
32. Dolzhenko P, Tikhonova M, Odnobokova M, Kaibyshev R, Belyakov A. Ultrafine-grained stainless steels after severe plastic deformation. *Metals*. 2023;13(4): 674.
33. Kaibyshev R, Mazurina I, Sitdikov O. Geometric dynamic recrystallization in an AA2219 alloy deformed to large strains at an elevated temperature. *Materials Science Forum*. 2004;467–470: 1199–1204.
34. Sitdikov O, Avtokratova E, Markushev M, Sakai T. Structural characterization of binary Al-Cu alloy processed by equal channel angular pressing at half of the melting point. *Metallurgical and Materials Transactions A*. 2023;54: 505–525.
35. Carreño F. Predicting ECAP misorientation evolution and its influence on superplasticity for an Al-Zn-Mg-Cu alloy. *Materials Research Proceedings*. 2023;32: 189–196.
36. Kim HS. Evaluation of strain rate during equal-channel angular pressing. *Journal of Materials Research*. 2002;17(01): 172–179.
37. *OIM Analysis Tutorials PDF – Scribd*. Available from: https://www.scribd.com/document/351952255/OIM-Analysis-Tutorials-pdf
38. *Channel 5 (Oxford Instruments HKL A/S 2007)*. Available from: https://alabama.app.box.com/s/6r4atfrtolhxh9dh1xk6twgutpr73dpi
39. Kaibyshev R, Sitdikov O, Mazurina I, Lesuer DR. Deformation behavior of a 2219 Al alloy. *Materials Science and Engineering: A*. 2002;334(1–2): 104–113.
40. Davis JR. *ASM Handbook: Nonferrous alloys and special-purpose materials. Vol. 2*. 10th ed. Ohio, USA: ASM International; 1990.
41. Belov NA, Akopyan TK, Shurkin PK, Korotkova NO. Comparative analysis of structure evolution and thermal stability of commercial AA2219 and model Al-2 wt%Mn-2 wt%Cu cold rolled alloys. *Journal of Alloys and Compounds*. 2021;864: 158823.
42. Blum W, McQueen HJ. Dynamics of recovery and recrystallization. *Materials Science Forum*. 1996;217–222: 31–42.
43. Blum W, Zhu QS, Merkel R, McQueen HJ. Evolution of grain structure in hot torsion of Al-5Mg-0.7Mn (AA5083). *Materials Science Forum*. 1996;217–222: 611–616.
44. McQueen HJ, Blum W. Recovery and recrystallization in aluminum alloys: Fundamentals and practical applications. In: *Proceedings of the 6th International Conference on Aluminium Alloys*. 1998. p.99–112.
45. McQueen HJ, Spigarelli S, Kassner ME, Evangelista E. *Hot deformation and processing of aluminum alloys*. 1st ed. Boca Raton: CRC Press; 2011.
46. Kuhlmann-Wilsdorf D. "Regular" deformation bands (DBs) and the LEDS hypothesis. *Acta Materialia*. 1999;47(6): 1697–1712.
47. Hurley PJ, Humphreys FJ. The application of EBSD to the study of substructural development in a cold rolled single-phase aluminium alloy. *Acta Materialia*. 2003;51(4): 1087–1102.
48. Wang J, Kang S-B, Kim H-W. Shear features during equal channel angular pressing of a lamellae eutectic alloy. *Materials Science and Engineering: A*. 2004;383(2): 356–361.
49. Utyashev FZ, Raab GI. Influence of large and severe plastic deformation mechanisms on structure formation in metals. *Materials Letters*. 2021;302: 130241.
50. Duckham A, Knutsen RD, Engler O. Influence of deformation variables on the formation of copper-type shear bands in Al–1Mg. *Acta Materialia*. 2001;49(14): 2739–2749.